Journal of Environmental Radioactivity 139 (2015) 185–199

Contents lists available at ScienceDirect

Journal of Environmental Radioactivity

journal homepage: www.elsevier.com/locate/jenvrad

JMA's regional atmospheric transport model calculations for the WMO technical task team on meteorological analyses for Fukushima Daiichi Nuclear Power Plant accident

Kazuo Saito [a,*], Toshiki Shimbori [a], Roland Draxler [b]

[a] JMA Meteorological Research Institute, 1-1, Nagamine, Tsukuba, Ibaraki 305-0052, Japan
[b] NOAA Air Resources Laboratory, College Park, MD, USA

ARTICLE INFO

Article history:
Received 2 October 2013
Received in revised form
25 January 2014
Accepted 10 February 2014
Available online 3 April 2014

Keywords:
Fukushima
Deposition
Air concentration
Atmospheric transport model
Cesium
WMO

ABSTRACT

The World Meteorological Organization (WMO) convened a small technical task team of experts to produce a set of meteorological analyses to drive atmospheric transport, dispersion and deposition models (ATDMs) for the United Nations Scientific Committee on the Effects of Atomic Radiation's assessment of the Fukushima Daiichi Nuclear Power Plant (DNPP) accident. The Japan Meteorological Agency (JMA) collaborated with the WMO task team as the regional specialized meteorological center of the country where the accident occurred, and provided its operational 5-km resolution mesoscale (MESO) analysis and its 1-km resolution radar/rain gauge-analyzed precipitation (RAP) data. The JMA's mesoscale tracer transport model was modified to a regional ATDM for radionuclides (RATM), which included newly implemented algorithms for dry deposition, wet scavenging, and gravitational settling of radionuclide aerosol particles.

Preliminary and revised calculations of the JMA-RATM were conducted according to the task team's protocol. Verification against Cesium 137 (^{137}Cs) deposition measurements and observed air concentration time series showed that the performance of RATM with MESO data was significantly improved by the revisions to the model. The use of RAP data improved the ^{137}Cs deposition pattern but not the time series of air concentrations at Tokai-mura compared with calculations just using the MESO data.

Sensitivity tests of some of the more uncertain parameters were conducted to determine their impacts on ATDM calculations, and the dispersion and deposition of radionuclides on 15 March 2011, the period of some of the largest emissions and deposition to the land areas of Japan. The area with high deposition in the northwest of Fukushima DNPP and the hotspot in the central part of Fukushima prefecture were primarily formed by wet scavenging influenced by the orographic effect of the mountainous area in the west of the Fukushima prefecture.

1. Introduction

The 2011 earthquake off the Pacific coast of Tōhoku (Great East Japan Earthquake) and tsunami occurred on 11 March 2011 and caused severe damage in Japan. The United Nations Scientific Committee on the Effects of Atomic Radiation (UNSCEAR) was asked to produce a scientific report for the General Assembly on the levels and effects of radiation exposure due to the accident at the Fukushima Daiichi Nuclear Power Plant (DNPP), and requested that the World Meteorological Organization (WMO) develop a set of meteorological analyses for assessing the atmospheric transport, dispersion and deposition of radionuclear materials. WMO convened a technical task team of experts from five countries (Austria, Canada, Japan, United Kingdom, and the United States) in November 2011 responding to UNSCEAR's request (Draxler et al., 2014). The primary aim of the group was to examine how the use of meteorological analyses could improve the atmospheric transport, dispersion and deposition model (ATDM) calculations.

The Japan Meteorological Agency (JMA) collaborated with the WMO task team as a regional specialized meteorological center (RSMC) of the country in which the accident occurred, and provided its operational 4D-VAR mesoscale (MESO) analysis and radar/rain gauge-analyzed precipitation (RAP) data in the WMO standard format (GRIB2). To evaluate the quality of meteorological analyses, the WMO task team conducted test simulations of their regional

* Corresponding author. Tel.: +81 298538630; fax: +81 298538649.
E-mail address: ksaito@mri-jma.go.jp (K. Saito).

http://dx.doi.org/10.1016/j.jenvrad.2014.02.007

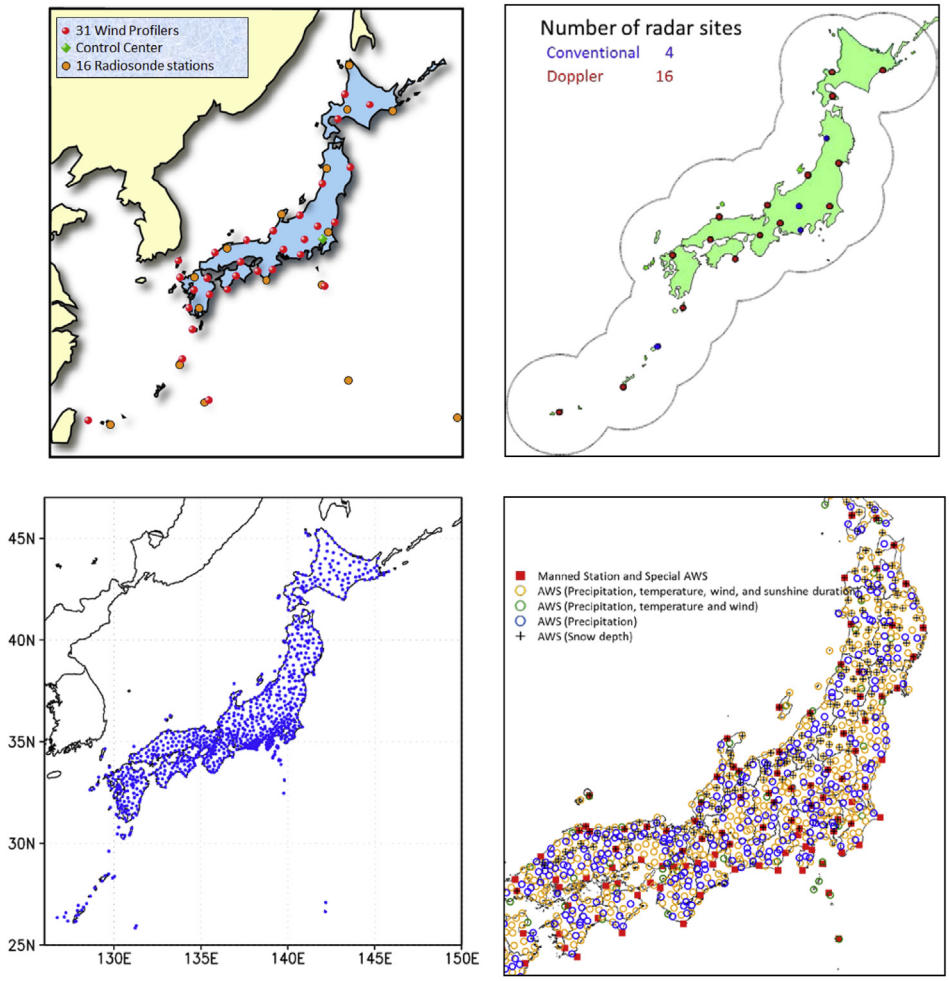

Fig. 1. Observations used in JMA-MESO and RAP. Upper left: upper air observations by JMA. Upper right: radar observations by JMA (as of March 2011). Lower left: GPS stations of GSI. Lower right: Surface observations by JMA.

ATDMs with different meteorological analyses. JMA modified its operational regional atmospheric transport model (RATM) for the predictions of oxidant concentration and volcanic-ash fall quantity, and developed a regional ATDM for radionuclides by newly implementing dry deposition, wet scavenging, and gravitational settling of radionuclide aerosol particles[1] (hereafter, referred as 'JMA-RATM'). Preliminary and revised calculations of JMA-RATM were conducted according to the Task Team's protocols with a horizontal concentration and deposition grid resolution of 5 km using a unit source emission rate.

This paper describes JMA's contribution to the task team effort, the development of JMA-RATM, and its application to the regional ATDM calculations from Fukushima DNPP. The organization of this paper is as follows. In Section 2, JMA's contributions to the WMO Task Team are briefly introduced, and the operational MESO analysis and RAP data are described including a data conversion tool prepared by JMA to read these data. In Section 3, JMA-RATM is briefly introduced and the modifications required for radionuclide simulations are presented. Section 4 shows the result of the ATDM calculation, and verification against ^{137}Cs deposition measurements and air concentration time series based on the Task Team protocols. The overall results are discussed in Section 5. Impacts of ATDM parameters such as release height, wet scavenging application height, below-cloud scavenging coefficient, dry deposition application height and number of computational particles are shown by sensitivity tests. The dispersion and deposition of radionuclides on 15 March 2011, the period of some of the largest emissions and deposition to the land areas of Japan is discussed. Further revisions of JMA-RATM relevant to the ATDM intercomparison by the Science Council of Japan (SCJ) are described. Summary and concluding remarks are given in Section 6.

2. JMA's contributions to WMO task team

2.1. MESO analysis of JMA

To assist in the regional ATDM calculations, JMA provided their MESO analyses fields to the WMO Task Team and UNSCEAR for the period 11 to 31 March 2011, at 3-hourly intervals and at a 5-km horizontal resolution. The MESO analyses are produced by an operational JMA regional nonhydrostatic 4D-VAR system (JNoVA; Honda et al., 2005; Honda and Sawada, 2008), which assimilates a variety of local meteorological observations, including 16 radio sondes and 31 wind profilers (upper left panel of Fig. 1), Doppler radial winds from 16 JMA C-band radars (upper right),[2] total

[1] Light particles composed of radioactive matter or other accumulation-mode aerosol particles carrying some radioactive matter.

[2] As of March 2011, four of the C-band JMA radars were conventional, while these radars have been replaced by Doppler ones since March 2013.

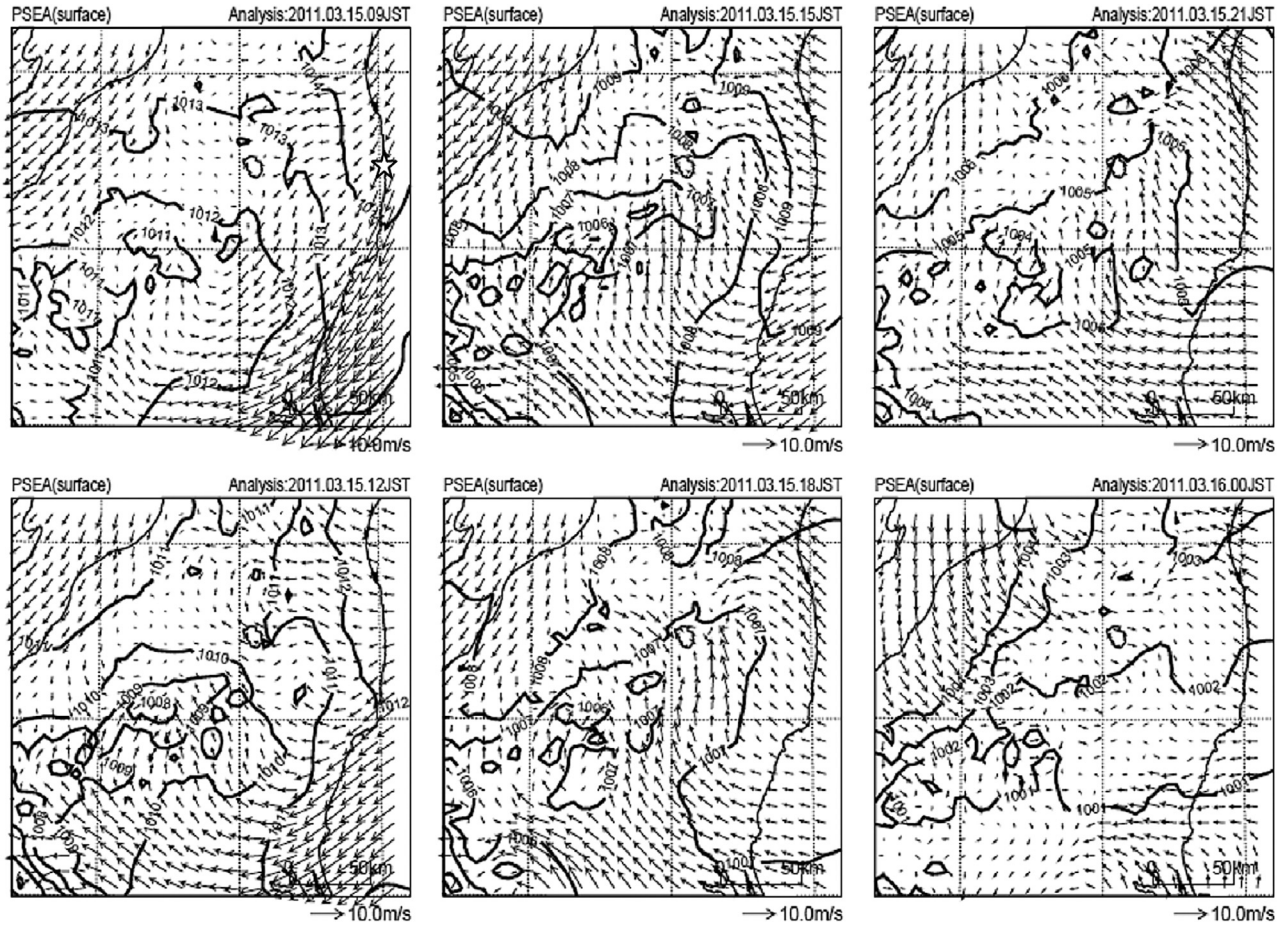

Fig. 2. Winds (950 hPa) (arrows) and mean sea level pressure (contour) by JMA-MESO for 15 March 0000 UTC (0900 JST)–1500 UTC (2400 JST). Star symbol in the upper left panel indicates the location of Fukushima DNPP.

precipitable water vapor derived from 1200 GPS stations of the Geospatial Information Authority of Japan (GSI, lower left). One of the unique features of JMA-MESO analysis is that the JMA-RAP data, based on the JMA radar network and surface observations (lower right, for more details on RAP, see Section 2.2), is also assimilated in the 4D-VAR (Koizumi et al., 2005). These data are assimilated in hourly time slots in the 3-h data assimilation windows by the inner loop (tangent linear/adjoint) model with a horizontal resolution of 15 km, and all analysis fields including liquid and solid precipitation are produced by a 3-h forecast of the non-linear outer-loop model (JMA nonhydrostatic model (JMA-NHM); Saito et al., 2006, 2007; 2012) of the incremental 4D-VAR with a horizontal resolution of 5 km. The JMA-MESO covers Japan and its surrounding area by 719 (x-direction) $\times$ 575 (y-direction) grid points on a Lambert Conformal projection (see Fig. 1 of Draxler et al. (2014)) up to about 21 km above ground level (AGL). There are 50 vertical levels, including 11 levels below 1 km AGL. Although the original horizontal and vertical grid configurations of the JMA-Mesoscale model and JNoVA 4D-VAR analysis are Arakawa-C and Lorentz types, respectively, for handling simplicity all data on the staggered points (horizontal and vertical wind speeds) are interpolated to the scalar points in the data provided to the Task Team.

Fig. 2 shows the time evolution of 950 hPa winds and mean sea level pressure by JMA-MESO for 15 March 2011, the date on which the largest emission of radionuclides from the Fukushima DNPP was observed (see Fig. 6). As discussed in Chen et al. (2011), from March 14th to 15th a weak low pressure trough moved eastward off the southern coast of the main island of Japan and then moved toward the northeast while developing rapidly after the 15th. Weak precipitation was observed in the Fukushima prefecture during the night from 0800 UTC (1700 JST) to 1900 UTC (0400 JST on 16th), March 15th (Kinoshita et al., 2011). The low level winds of JMA-MESO around Fukushima DNPP were westerly until the day before (the 14th), but changed to north-northeasterly during the morning of the 15th. After 0600 UTC (1500 JST), the winds turned east-southeasterly, and caused the critical deposition episode over the Fukushima prefecture. Fig. 3 shows the 1-h average surface precipitation by JMA-MESO for 15 March 1200–1500 UTC. Most of the surface precipitation over northern Japan during this period was in the form of snow (center panel) except in some of the coastal areas.

2.2. Radar/rain gauge-analyzed precipitation (RAP)

JMA also provided the RAP dataset at 30 min intervals, with a horizontal resolution of 45 s (about 1.11 km) in longitude and 30 s (about 0.93 km) in latitude covering a region from 118 to 150°E and from 20 to 48°N (2560 by 3360 grid points). JMA produces RAP by calibrating radar echo data with 1-h accumulated rain gauge precipitation data. In addition to the JMA network of 20 C-band radars and 1300 surface observations (Fig. 1), echo data from an additional 26 C-band radars operated by the Ministry of Land, Infrastructure, Transport and Tourism and precipitation data from an additional 8700 rain gauges in Japan are collected in the real-time operation. A more detailed description of the RAP processing is found in Nagata (2011).

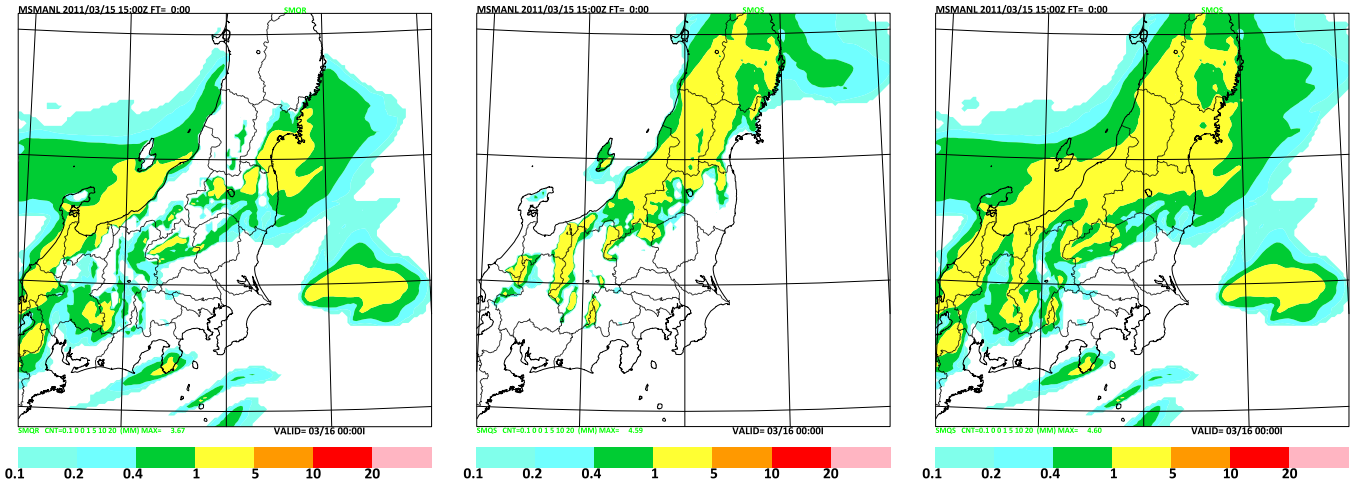

Fig. 3. Accumulated surface precipitation (mm per hour) by JMA-MESO for 15 March 1200–1500 UTC. Rain (left), snow (center) and total precipitation (right).

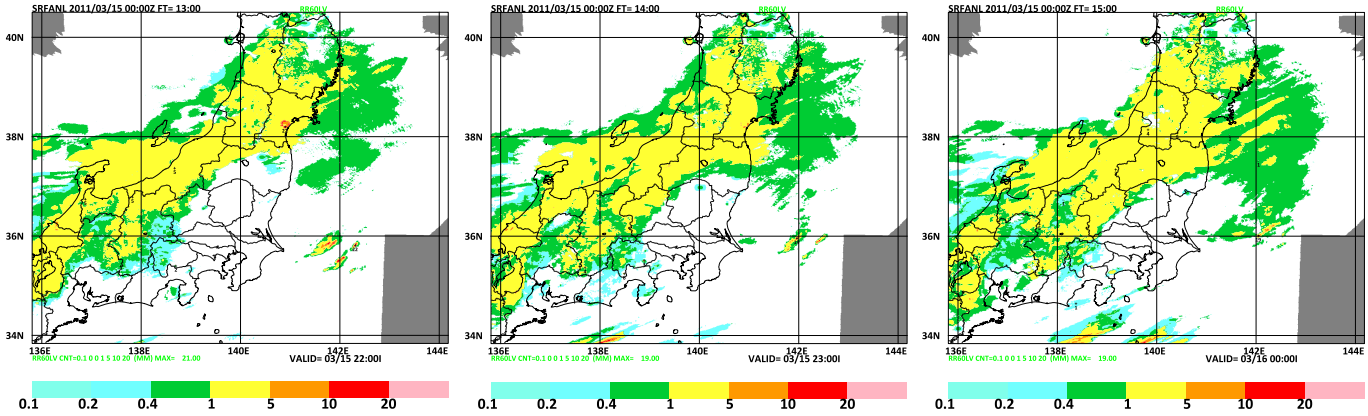

Fig. 4. Rainfall intensity (mm) by JMA-RAP for 15 March. 1200–1300 UTC (left), 1300–1400 UTC (center) and 1400–1500 UTC (right). Color shade corresponds to Fig. 3.

JMA-RAP intensities at 1-h intervals for 15 March 1200–1500 UTC are shown in Fig. 4. This illustrates a good agreement[3] of RAP with the JMA-MESO total precipitation (right panel of Fig. 3). A circle-shaped very small intense precipitation area is seen around the radar site at Sendai (38.3N, 140.9E) for 1200–1300 UTC (left), which is due to a bright band observed by the Sendai radar. A documentation of GRIB2 format of RAP data is given by Toyoda (2012).

2.3. File converter kit

JMA provided the MESO and RAP data in GRIB2 format to members of the Task Team and UNSCEAR group B. The MESO data are on a Lambert conformal projection in the horizontal coordinate and a terrain-following hybrid vertical coordinate. Furthermore, while the GRIB2 format is defined by WMO as a common format to exchange meteorological data, for some users it is not an easy task to decode and process GRIB2. Considering the situation, JMA provided a software tool to read and process the MESO and RAP data (Chen et al., 2012a,b). This file converter tool is a UNIX software kit (JMA, 2012) and provides the following three functions:

(i) converts the GRIB2 format data to the FORTRAN sequential binary format data (GrADS),
(ii) re-projects the data from the Lambert conformal projection to a regular latitude–longitude projection, and
(iii) converts the data from terrain-following hybrid vertical coordinates to an isobaric coordinate at user-specified pressure surfaces.

Both the JMA-MESO and RAP data, detailed instructions, and the above mentioned file converter kit were made available to the UNSCEAR community through a WMO hosted password protected FTP site. The data are also available to the scientific community for research purposes provided that JMA is acknowledged as the data source. Researchers should contact WMO (dpfsmail@wmo.int).

For more details on the JMA's contributions to the WMO Task Team, the meteorological data, and the file conversion kit, see Saito et al. (2014).

3. JMA-RATM

3.1. Brief description of JMA-RATM

The JMA-RATM is a mesoscale tracer transport model, which can be driven by the MESO analysis data. The model takes a Lagrangian scheme (Iwasaki et al., 1998; Seino et al., 2004) with many computational particles that follow advection, horizontal and vertical diffusion, gravitational settling, dry deposition and wet

[3] In MESO analysis, RAP data are assimilated through minimization of the cost function of 4D-VAR, but MESO precipitation sometimes disagrees with RAP when the other terms in the cost function prevails or the outer-loop model in 4D-VAR cannot reproduce the observed rainfall (typically, intense convective rains).

scavenging processes. The RATM was originally developed at JMA for photochemical oxidant predictions (Takano et al., 2007) and volcanic-ash fall forecasts (Shimbori et al., 2009) in Japan. The details of the original RATM have been described by Shimbori et al. (2010).

Because the original RATM of JMA was not applied in predicting the dispersion and deposition of radionuclides, the deposition schemes needed to be modified. For the wet deposition of radionuclide aerosol particles, only washout processes (below-cloud scavenging) are considered. The below-cloud scavenging rate is given by Kitada (1994) (red solid line of Fig. 12)[4]:

$$\Lambda_w = AP^B, \tag{1}$$

$$A = 2.98 \times 10^{-5}\mathrm{s}^{-1}, \quad B = 0.75, \tag{2}$$

where P is the precipitation intensity [mm h^{-1}] given by the 3-h average of the accumulated precipitation from the MESO analyses or every 30 min from the RAP data.

On the other hand, wet deposition for a depositing gas (*e.g.*, ^{131}I) is considered only as a rainout process (in-cloud scavenging). The in-cloud scavenging rate is given by Hertel et al. (1995):

$$\Lambda_r = \frac{1}{(1-\mathrm{LWC})/HRT_a + \mathrm{LWC}} \frac{P}{Z_r}, \tag{3}$$

where LWC is the liquid water content, H the Henry's constant (=0.08 M atm^{-1}; Draxler et al. (2013)), R the ideal-gas constant (=0.082 atm M^{-1} K^{-1}), T_a the temperature [K], and Z_r is the height over which in-cloud scavenging takes place. LWC, T_a, and Z_r can be defined by the MESO data which include amount of cloud water and rain.

Wet scavenging is applied to computational particles or gases under the height of about 3000 m (ASL) in the original RATM (Shimbori et al., 2010). Verification results for the gaseous ^{131}I deposition computation is given in Draxler et al. (2013), while only the results for the ^{137}Cs aerosol particles are discussed in this paper.

Dry deposition is simply computed from the following deposition rate (*e.g.*, Iwasaki et al., 1998):

$$\Lambda_d = \frac{V_d}{Z_d}, \tag{4}$$

where V_d is the dry-deposition velocity and Z_d is the depth of surface layer. The value of V_d is set to 0.001 m s^{-1} for aerosol particles and 0.01 m s^{-1} for depositing gas (Sportisse, 2007; Draxler and Rolph, 2012), and Z_d is set to 100 m for both tracer types.

Furthermore, gravitational settling is considered for aerosol particles in the vertical advection step. These computational particles follow the Stokes' law with a slip correction and the terminal velocity is given by (*e.g.*, Sportisse, 2007)

$$V_t = \frac{1}{18}\frac{D^2\rho_p g}{\eta_a} C_c, \tag{5}$$

where C_c is the Cunningham correction factor:

$$C_c = 1 + \frac{2\lambda_a}{D}\left[a + b\exp\left(-c\frac{D}{2\lambda_a}\right)\right], \tag{6}$$

with $a = 1.257$, $b = 0.400$ and $c = 1.100$. The mean free path of air λ_a in Eq. (6) is calculated by

$$\lambda_a = \lambda_0 \frac{\eta_a p_0}{\eta_0 p_a}\left(\frac{T_a}{T_0}\right)^{1/2}, \tag{7}$$

where η_a is the viscosity of air, p_a is the atmospheric pressure, and $\eta_0 = 18.2$ μPa s, $\lambda_0 = 0.0662$ μm are the corresponding values for the reference atmosphere ($T_0 = 293.15$ K, $p_0 = 1013.25$ hPa). The distribution of particle size D is assumed to be log-normal with mean diameter of 1 μm and standard deviation of 1.0 (upper cutoff: 20 μm), with a uniform particle density ρ_p of 1 g cm^{-3}. Note that if a computational particle moves under the model surface by the vertical advection or diffusion, it is numerically reflected to the mirror symmetric point above the surface.

Specifications of the original and the preliminary version of JMA-RATM are summarized in Table 1.

3.2. Use of MESO and RAP data

The motion of computational particles in JMA-RATM is calculated in the same coordinate system as the MESO analysis (Lambert conformal in the horizontal and a terrain-following hybrid in the vertical). For the wet deposition process, due to limitations in the treatment of ice phase deposition in the RATM, only liquid rain (left panel of Fig. 3) was considered in the Task Team calculation. We will show the result using the total precipitation (right panel of Fig. 3) in Section 5.3.

Table 1
Specifications of JMA-RATM.

	Original version (for volcanic -ash)	Preliminary version	Revised version
Meteorological field	Hourly outputs of JMA-MESO forecast	Three-hourly outputs of JMA-MESO analysis	Same as left
Grid size	5 km	5 km	5 km
Number of particles	100,000/ 10 min	100,000/3 h	300,000/3 h
Time step	3 min	10 min	10 min
Horizontal diffusion	Gifford (1982, 1984)	Same as left	Same as left
Vertical diffusion	Louis et al. (1982)	Same as left	Same as left
Dry deposition	Vpar: $V_d = 0.3$ m s^{-1}	Ngas: N/A Dgas: $V_d = 0.01$ m s^{-1} Lpar: $V_d = 0.001$ m s^{-1}	Ngas: N/A Dgas: same as left Lpar: same as left
Wet scavenging	Vpar: Kitada (1994) with MESO forecast	Ngas: N/A Dgas: Hertel et al. (1995) Lpar: Kitada (1994) with MESO analysis or RAP data below 3000 m (ASL)	Ngas: N/A Dgas: same as left Lpar: same as left except height level is below 1500 m (ASL)
Gravitational settling	Vpar: Suzuki (1983)	Ngas: N/A Dgas: N/A Lpar: Stokes' law with Cunningham correction	Ngas: N/A Dgas: N/A Lpar: same as left
Reflection on the ground	N/A	Iwasaki et al. (1998)	Same as left
Decay	N/A	Half-lifetime	Same as left

Ngas: noble gas, Dgas: depositing gas, Lpar: light radionuclide aerosol particle, Vpar: volcanic-ash particle.

[4] The value of the coefficient A as it appeared in the first equation in Section 4.4 on JMA-RATM of the WMO report (Draxler et al., 2013) (2.78×10^{-5}) is misspelled.

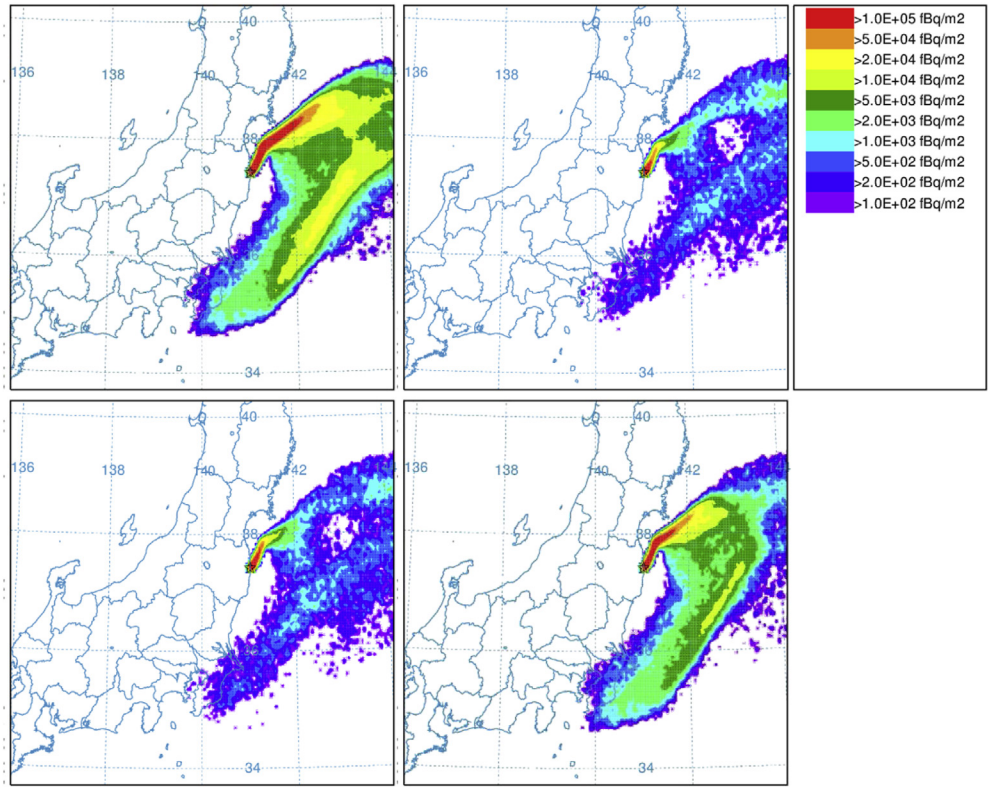

Fig. 5. Aerosol particle accumulated deposition by the JMA-RATM for unit release (1 Bq/h) at 14 March 0000–0300 UTC. JMA-MESO is used for precipitation. Upper left: without vertical advection. Upper right: vertical motion is computed by updraft/downdraft. Lower left: 9-grid average was applied. Lower right: 9-grid average and $w^* = 0$ at the lowest level. Note that unit in the color bar is fBq (femto Becquerel) per square meters. See text for details of the different calculations.

When using the RAP data, instead of the 3-hourly accumulated precipitation by MESO, the RAP precipitation intensity at each MESO grid point (5-km horizontal resolution) is calculated from the spatial average of the surrounding 25-grid cells of RAP (1-km resolution) every 30 min. As noted above, because RATM cannot treat ice phase deposition and RAP does not distinguish solid and liquid precipitations, all RAP precipitation was considered to be liquid rain in the calculation.

3.3. Revision of RATM

As previously mentioned, the JMA-MESO analysis is produced by a 3 h forecast of the outer-loop model (JMA-NHM with a horizontal resolution of 5 km) of 4D-VAR. The stored values in the analysis field are not averaged in the assimilation window but are the instantaneous values predicted by the outer-loop model at the analysis time (the end of each 3-h assimilation window). Because the instantaneous vertical motion is affected by gravity waves and short-lived convection, a simple time interpolation of updrafts/downdrafts between the three-hourly analysis fields may yield an overestimation of the vertical advection of the air parcel, even if the magnitude of updrafts/downdrafts is small.

To compensate for the lack of temporal resolution, in the revised version of RATM, the vertical advection is calculated using a spatially-averaged (9-grid cells) value of the MESO vertical velocity and the vertical motion is assumed to be terrain-following ($w^* = 0$) at the lowest model level (40 m).[5] Fig. 5 compares 24-h ^{137}Cs accumulated deposition for unit release (1 Bq/h) from 0000 to 0300 UTC, 14 March. The upper right panel shows the result where vertical motion of the particles is computed using the original MESO vertical velocity. Compared to the case without vertical advection (upper left), the deposition over the sea off the east coast of Japan is reduced. The lower-left panel provides the result when the 9-grid cell averaged updraft/downdraft was applied to compute the vertical advection. The difference from the upper right panel is not large but the deposition is slightly increased near the source point and slightly decreased at distant areas. In these simulations, aerosol particles emitted from the source point were first lifted up by the lowest level's small updraft in MESO. The lower right panel is the result of when the lowest level vertical motion was assumed to be terrain following (*i.e.*, the lowest level updraft/downdraft becomes zero over sea while the remaining vertical motion corresponds to the terrain slope and the horizontal wind speed). The deposition off the east coast of Japan is increased.

In the preliminary version of RATM, wet scavenging was assumed to occur below about 3000 m in height, the same as in the original RATM (Section 3.1), but deposition over Miyagi prefecture, to the north of Fukushima, was overestimated compared with the aircraft monitoring by the Ministry of Education, Culture, Sports, Science and Technology of Japan (MEXT) (Fig. 4 of Draxler et al., 2013). In the revised RATM, this overestimation was reduced by limiting the level of wet scavenging to levels below about 1500 m (see Sections 4.1 and 5.1.2).

Some improper treatments of horizontal and vertical interpolations of the kinematic fields were found in the preliminary version of RATM. These computational bugs were corrected in the

[5] This relationship is held rigorously at the surface in the terrain-following coordinate as the lower boundary condition. Here, we applied this condition to the lowest level of the ATM for the deposition calculation when the 3-h mesoscale analysis data are temporally interpolated. Note that most meteorological analyses lack the vertical motion field but the JMA-MESO analysis contains the vertical motion as computed by the outer-loop model of 4D-VAR.

revised version. Also the number of computational particles was increased from 100,000/3 h to 300,000/3 h, but the impact was almost negligible (see Section 5.1.3).

4. RATM runs and verification

4.1. Experimental setting

According to the computational framework described in Annex VII of Chen et al. (2011) and Draxler et al. (2014), ATDM simulations were conducted by the WMO task team for the computational period of 11 March 1800 UTC through 31 March 2400 UTC, in three-hourly emission period increments using a unit source rate (1 Bq/h) for each discrete emission time segment. Emissions were uniformly distributed from the ground surface to 100 m AGL, and the concentration or deposition at any grid cell in the domain was given by the sum of the contribution from each ATDM emission segment after multiplying the resulting unit concentrations by the emission rate for each segment (Draxler and Rolph, 2012). The ATDM air concentration and deposition output fields were configured to use a regular latitude–longitude grid (601 by 401 grid cells) with the output averaged at three-hourly intervals at 0.05° (5 km) horizontal resolution and 100 m vertical resolution. In the post-processing step, the results from each of the 168 ATDM simulations were multiplied by the actual emission rate at the release time of the simulation and decay constant for each radionuclide thereby permitting the same ATDM dispersion and deposition factors to be applied to multiple radionuclides. The estimated emission rates by the Japan Atomic Energy Agency (JAEA; broken line in Fig. 6), originally derived by Chino et al. (2011) and later modified by Terada et al. (2012) were used for the simulations.

Fig. 7 compares ^{137}Cs accumulated deposition for 11 March to 3 April 2011 estimated using different computational methodologies. Here, rain in JMA-MESO was used for the calculations shown in the left panels while RAP data were used for those shown in the right panels. In the preliminary version RATM (upper figures), deposition over Miyagi prefecture (north of Fukushima) and southern part of the Kanto Plain (west of Tokyo) was overestimated compared with observation as mentioned in the previous Section 3.3. In the revised RATM (lower figures), this overestimation was ameliorated. When RAP data is used for precipitation, an area with high deposition in the northwest of Fukushima DNPP becomes more distinctly reproduced (right figures), but the overestimation of deposition in the southern part of the Kanto Plain is also enhanced, even in the revised RATM.

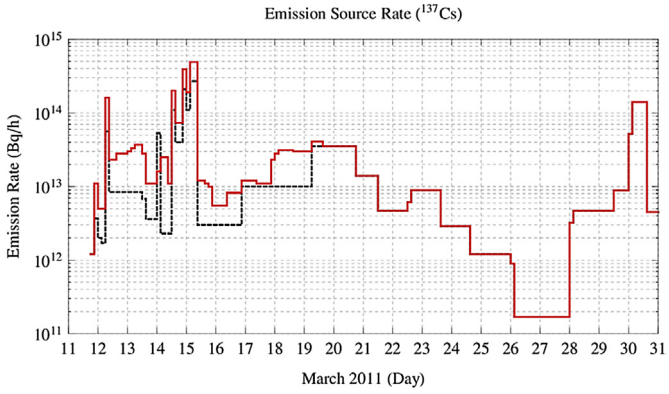

Fig. 6. The time varying emissions in Becquerel per hour at 3 h intervals for ^{137}Cs used for the ATDM-meteorology evaluations at the WMO task team (JAEA; black broken line), and SCJ simulation (JAEA2; red solid line). (For interpretation of the references to color in this figure legend, the reader is referred to the web version of this article.)

4.2. Verifications against observation

The ^{137}Cs dispersion and deposition were verified against the observed time series of near ground level air concentrations at Tokai-mura (JAEA) and measurements taken by the U.S. Department of Energy's (USDOE, 2011) fixed-wing aircraft (C-12) from 2 April 2011 to 9 May 2011 and ground based measurements by MEXT (2011). The collected aircraft and ground based data points were averaged onto an identical grid (0.05° resolution) to that used in the ATDM calculations (Draxler et al., 2013). Fig. 8 shows the ^{137}Cs deposition used for verification and location of Tokai-mura (JAEA). One of the characteristic features of the deposition pattern is the densely contaminated area extending to northwest from Fukushima DNPP. This area is bent to the south, east of O'u mountain range, and forms an inverse L-shaped pattern shown by the yellow shaded region. On the other hand, deposition in Miyagi prefecture, north of Fukushima, is relatively small.

The following statistical metrics used in Draxler et al. (2013) were applied to the results of the preliminary and revised RATMs.

(i) Correlation coefficient (R), the scatter among paired measured and predicted values.
(ii) The fractional bias (FB), a normalized measure of bias.
(iii) Figure of merit in space (FMS), the percentage of overlap between measured and predicted areas.
(iv) Kolmogorov–Smirnov parameter (KSP), the maximum difference between two cumulative distributions.

A ranking method (Draxler, 2006) was defined by giving equal weight to the normalized expressions of these four statistical metrics,

$$\mathrm{METRIC1} = R^2 + 1 - |\mathrm{FB}/2| + \mathrm{FMS}/100 + (1 - \mathrm{KSP}/100), \tag{8}$$

whose value would range from 0 to 4 (from worst to best). Two additional spatial metrics are used in Draxler et al. (2013):

(v) Percentage of factor of two (%FA2), the percentage of calculations within a certain factor of two of the measured value.
(vi) Factor of exceedance (FOEX), the factor of the number of over-predictions in the pairs of predicted and measured values.

to define the following other metrics:

$$\begin{aligned} \mathrm{METRIC2} &= R^2 + 1 - |\mathrm{FB}/2| + \mathrm{FA2}/100 + (1 - \mathrm{KSP}/100), \\ \mathrm{METRIC3} &= \mathrm{METRIC1} + (1 - |\mathrm{FOEX}/50|), \\ \mathrm{METRIC4} &= \mathrm{METRIC3} + \mathrm{FA2}/100. \end{aligned} \tag{9}$$

The release rates estimated by JAEA (Terada et al., 2012; broken line in Fig. 6) are used for the calculations. Two sets of calculations were examined, where the precipitation was given by the MESO or the RAP data.

Table 2 shows verification statistics by JMA-RATMs for ^{137}Cs deposition. Performance of the revised RATM (Rev. MESO) is significantly improved compared with the preliminary version of RATM (Pre. MESO) for all rank metrics. The most improvement was obtained in the correlation coefficient (R), which increased from 0.45 in the preliminary version to 0.70 in the revised version. The use of RAP data for precipitation further improved the correlation coefficient to 0.84, while rank metrics became slightly worse due to the deterioration of fractional bias (FB) and factor of exceedance (FOEX). These tendencies in the statistics in the use of RAP data can

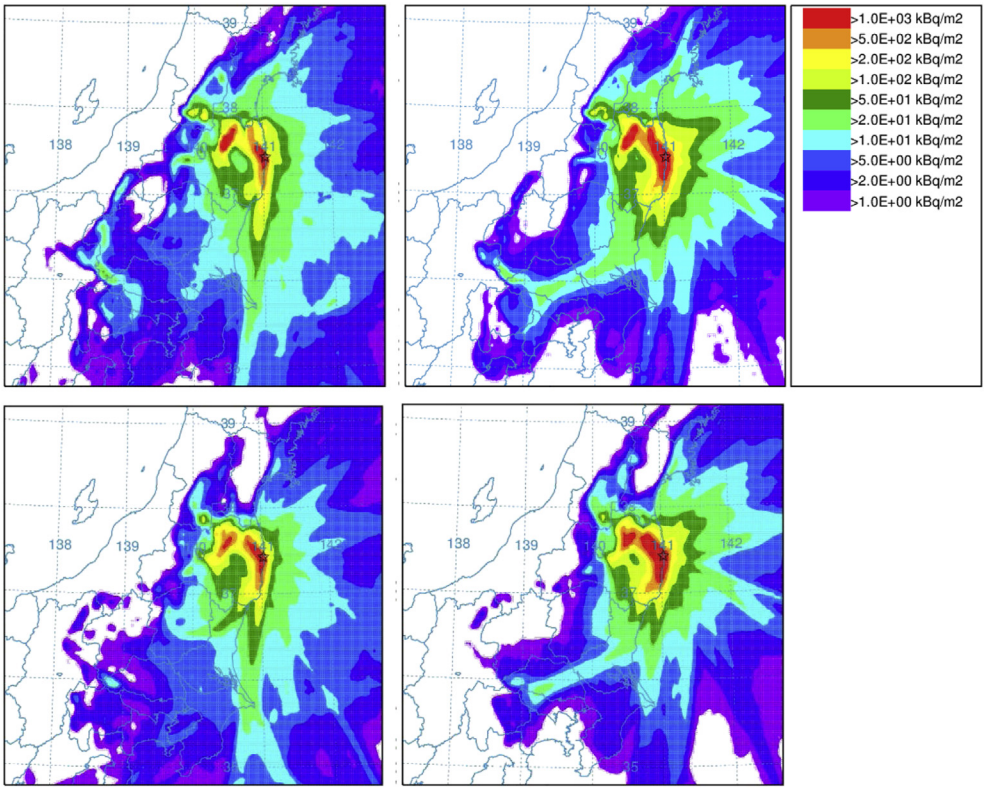

Fig. 7. ^{137}Cs accumulated deposition for 11 March–3 April 2011using the JAEA source. Upper left: preliminary RATM with MESO precipitation. Upper right: preliminary RATM with RAP precipitation. Lower: same as in upper figures but results by the revised RATM. Star symbols indicate the location of Fukushima DNPP.

be understood by the area with high deposition in the northwest of Fukushima DNPP and the overestimation of deposition in the west of the Kanto Plain in right panels of Fig. 7; in the aircraft monitoring by MEXT (Fig. 4 of Draxler et al., 2013), little or no deposition was observed in the western part of the Kanto Plain.

Fig. 9 and Table 3 show the time evolution and the corresponding statistics for ^{137}Cs concentration at the JAEA observation site. Performance of the revised RATM using MESO precipitation slightly improved in terms of the rank metrics, while the revision did not improve the metrics when the RAP data were used for precipitation. The reason for this deterioration in metrics in the use of RAP data is not obvious, but a similar tendency was also found in the other Task Team's ATDM experiments (Draxler et al., 2013, 2014). Arnold et al. (2014) inferred that the discrepancy of transport patterns by numerical weather prediction (NWP) analyses and the locations of the precipitation may result in a wrong description of the total wet scavenging. The quality of the RAP data itself is also arguable. Although the bright band (shown in Fig. 4) is not likely critical in this experiment, radar echoes are scanned around the level of 1 km AGL and solid waters are over-detected in the radar reflectivity. A lower limit of intensity around 0.4 mm h^{-1} is set in RAP, which means that very weak precipitation is not included. As mentioned in Section 3.2, all RAP precipitation was considered to be liquid rain in the wet scavenging calculation in JMA-RATM, and this assumption also may yield some errors in the time evolution. Another possibility is that dispersion of radionuclides to the position of the JAEA site is somewhat uncertain (Section 5.3). As suggested by Fig. 11 later, the southward advection of radionuclides from Fukushima DNPP on the March 15th was sensitive to small changes in the wind direction. Therefore, given the inherent limitations in the accuracy of wind direction in meteorological analyses, it may be unrealistic to expect that an ATDM can precisely reproduce the time evolution of downwind air concentrations at Tokai-mura. In addition, the statistical results may also be affected by remaining uncertainties in the radionuclides release rate estimates which may never be finalized.

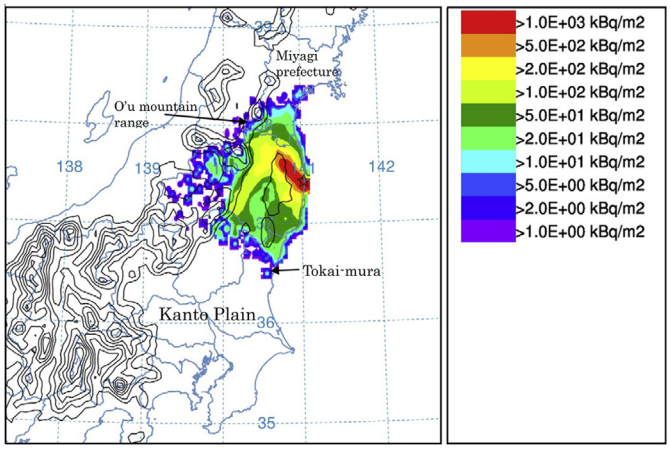

Fig. 8. Measured ^{137}Cs deposition based upon aerial and ground based sampling. The solid dark lines show the terrain contours at 250 m intervals (to 2000 m) as derived from the JMA-MESO analysis. Star symbol indicates the location of Fukushima DNPP. Reproduced from Draxler et al. (2013).

5. Discussion

5.1. Sensitivity experiments to RATM parameters

In the revision of JMA-RATM, we tested some parameters with the greatest uncertainty to determine their impacts on the ATDM calculations. Accumulated deposition patterns of ^{137}Cs from 11

Table 2
Metrics for comparison of JMA-RATM simulations with observed deposition pattern of ^{137}Cs using the JAEA source. Bold values indicate best score for each simulation.

RATM	*R*	FB	FMS (%)	FOEX (%)	%FA2 (%)	KSP	Metric 1	Metric 2	Metric 3	Metric 4
Pre. MESO	0.45	**−0.02**	**100.00**	**−0.46**	**51.01**	**10.0**	3.09	2.60	4.08	4.59
Pre. RAP	0.77	0.54	**100.00**	9.67	41.99	11.0	3.22	2.63	4.02	4.44
Rev. MESO	0.70	−0.04	99.63	−0.83	37.94	**10.0**	**3.37**	**2.75**	**4.35**	**4.73**
Rev. RAP	**0.84**	0.56	99.08	9.12	35.73	13.0	3.28	2.65	4.10	4.46

March 1800 UTC to 03 April 2100 UTC were compared. A list of values of parameters used in the experiments and corresponding figures is given in Table 4.

5.1.1. Release height

In the WMO Task Teams' experiments, emissions of radionuclides were assumed to be distributed uniformly from the ground to 100 m AGL. Although this release height was determined considering hydrogen explosions that occurred at the buildings of reactors No. 1, 3, and 4 of Fukushima DNPP, the height may change depending on the atmospheric conditions and situation of the emission. The substantial release of radionuclides on 15th March was not the result of a hydrogen explosion but caused by gradual emissions from various openings of the building of reactor No. 2 that were caused by the blast that occurred inside the building. In that case, the emission was likely confined within lower levels of the atmosphere.

The upper left panel of Fig. 10 shows the ^{137}Cs accumulated deposition when a lower release height (30 m) is applied. No significant difference was obtained in the dense deposited area compared with the case of the original release height (100 m; lower-left panel of Fig. 7). This general insensitivity to the release height in the deposition pattern is consistent with the calculation using the Models-3 Community Multiscale Air Quality (CMAQ)

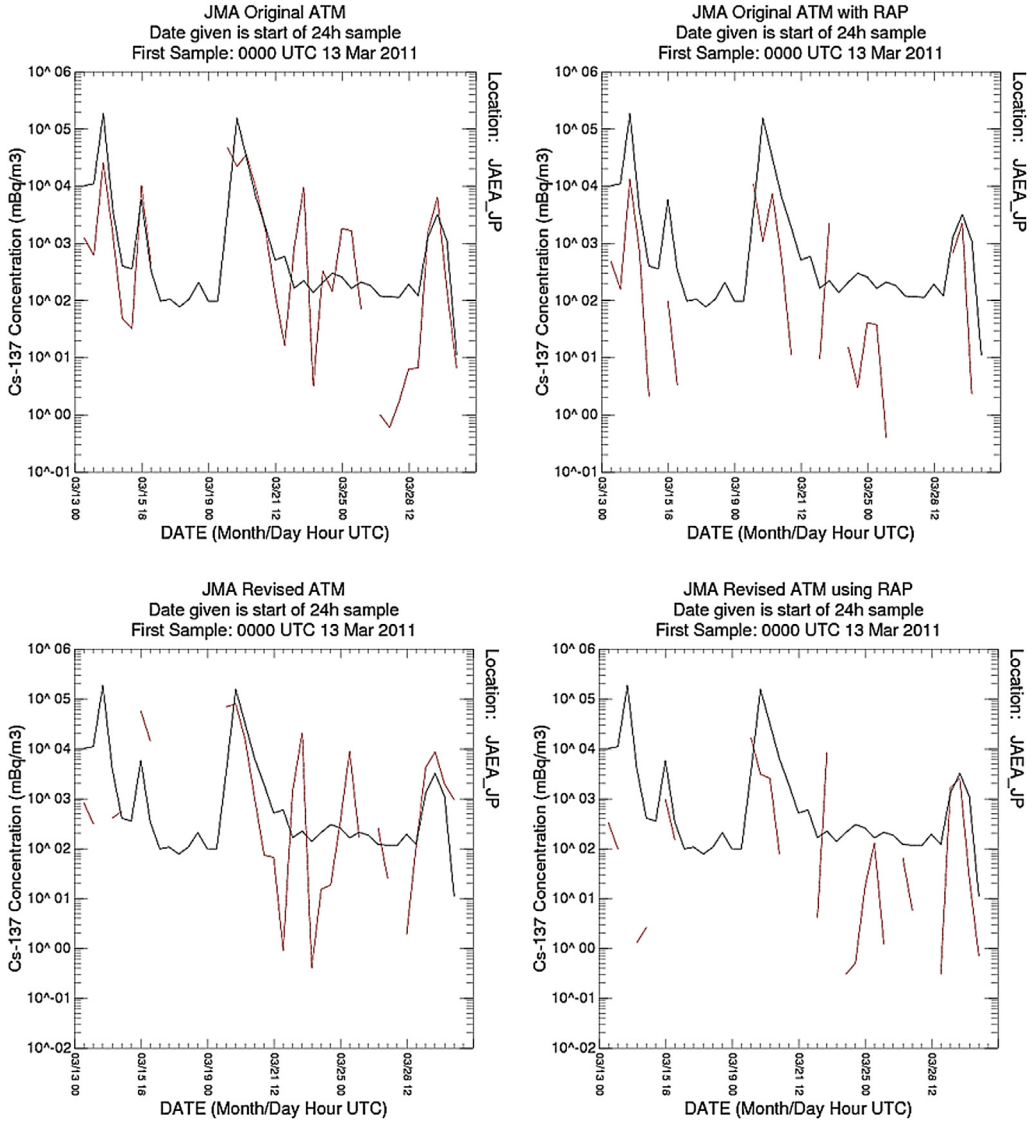

Fig. 9. Same as in Fig. 7 but time evolution of ^{137}Cs (logarithmic in the ordinate) at JAEA Tokai-mura for the period 13–31 March 2011. Black lines indicate observation. Red lines show results by JMA-RATM with the JAEA source estimation. (For interpretation of the references to color in this figure legend, the reader is referred to the web version of this article.)

Table 3
Metrics for comparison of JMA-RATM simulations with observed concentration time series of ^{137}Cs at Tokai-mura using the JAEA source. Bold values indicate best score for each simulation.

RATM	*R*	FB	FMS (%)	FOEX	%FA2 (%)	KSP	Metric 1	Metric 2	Metric 3	Metric 4
Pre. MESO	0.51	−0.82	**80.00**	−21.43	**21.43**	**43.0**	2.22	1.63	2.79	3.01
Pre. RAP	**0.59**	−1.66	57.50	−45.24	4.76	64.0	1.46	0.93	1.55	1.60
Rev. MESO	0.39	**−0.40**	77.5	**−19.05**	14.29	**43.0**	**2.30**	**1.67**	**2.92**	**3.06**
Rev. RAP	0.07	−1.68	62.5	−42.86	9.52	67.0	1.12	0.59	1.26	1.36

model by Morino et al. (2011). A small difference can be seen in the regions with weak deposition over southern part of the Kanto plain, where the simulated deposition becomes slightly smaller by using the lower release height. This change corresponds to the observed deposition pattern (see Fig. 4 of Draxler et al., 2013), and small hotspot northeast of Tokyo is vaguely simulated in this experiment.

5.1.2. Wet scavenging application height and coefficient

Wet scavenging is an important process for the deposition of radionuclides. The upper right panel of Fig. 10 indicates that when the wet scavenging process is not included in the simulation, the deposition becomes much less compared with the original calculation (lower-left panel of Fig. 7). This result shows that the area with high deposition in the northwest of Fukushima DNPP was strongly affected by wet scavenging. However the treatments of scavenging caused by rain and/or snow have many ambiguities. The original version of JMA-RATM considered wet scavenging below 3000 m with the scavenging coefficient of Eq. (2). The middle left panel of Fig. 10 shows the result with the original scavenging application height of 3000 m. A distinct difference from the original simulation is seen over the Miyagi prefecture, where overestimation of unobserved deposition is predicted. This result suggests that the wet scavenging should be confined in lower levels in the case of the Fukushima DNPP accident.

The middle right panel of Fig. 10 shows the sensitivity of the results to changes in the below-cloud scavenging coefficient. Here, the scavenging coefficient $\Lambda_w = 2.98 \times 10^{-5} P^{0.75}$ is replaced by $\Lambda_w = 8.40 \times 10^{-5} P^{0.79}$, the values used in UKMET-NAME (Leadbetter et al., 2014; red broken line of Fig. 12). When a lager value is applied, deposition of ^{137}Cs over west of the Kanto Plain is enhanced.

5.1.3. Dry deposition application height and number of computational particles

Sensitivities to dry deposition surface-layer height and number of computational particles were also examined. Using a lower dry deposition surface layer height $Z_d = 40$ m (the lowest model layer) had little impact on the deposition pattern (the lower-left panel of Fig. 10). The lower right panel of Fig. 10 shows the result when a smaller number of computational particles (100,000/3 h) were employed. Virtually the same result was obtained in the deposition patterns.

5.2. Dispersion and deposition of radionuclides on 15 March 2011

The most critical episode in the dispersion and deposition of radionuclides by the Fukushima DNPP accident was the inland deposition in the Fukushima prefecture on 15th March 2011. Radionuclides contaminated the area northwest of Fukushima DNPP, and spread to southwest along 'Naka-dori', the central part of the Fukushima prefecture extending from southwest to northeast in the east of the O'u mountain range (Fig. 8). Here, we discuss the deposition of radionuclides on 15th March from the RATM simulation.

The upper panel of Fig. 11 illustrates the three-hourly deposition of ^{137}Cs for the period from 15 March 0000 UTC to 16 March 0000 UTC by the three-hourly releases from 14 March 2100 UTC to 15 March 1200 UTC. As indicated by this figure, the main deposition northwest of Fukushima DNPP was produced during this period. The radionuclides released from 14th 2100 UTC to 15th 0000 UTC were first advected southward by the northnortheasterly low level wind (Fig. 2), and then changed direction to northwestward in the afternoon (after 0600 UTC) of the 15th. Blocked by the O'u mountain range, the atmospheric transport path of radionuclides turned and caused a secondary hotspot at 'Naka-dori' after 1200 UTC of the 15th. On the other hand, the radionuclides released from 0300 UTC to 0900 UTC of the 15th first directly spread northwest from Fukushima DNPP. As indicated in Fig. 6, the largest emission occurred in this period, and produced the area with high deposition northwest of the Fukushima DNPP. The atmospherically transported radionuclides were blocked by the O'u mountain range, again contributing to enhance the hotspot at 'Naka-dori', producing the inverse L-shaped pattern of deposition. The radionuclides released after 0900 UTC were advected southward and marginally detected at low air concentration levels at Tokai-mura.

The lower panel of Fig. 11 shows effect of wet scavenging (difference between wet scavenging off and on). Here, only positive

Table 4
List of values of parameters used in the experiments and corresponding figures.

Number of computational particles per 3 h	Release height (AGL) (m)	Time step (min)	Below-cloud scavenging coefficient for rain	Below-cloud scavenging coefficient for snow	Scavenging application height (ASL) (m)	Dry-deposition application height (AGL) (m)	Source emission	Figures
300,000	0–100	10	$A = 2.98 \times 10^{-5}$, $B = 0.75$	N/A	<1500	<100	JAEA	Lower-left of Fig. 7
300,000	0–30	10	$A = 2.98 \times 10^{-5}$, $B = 0.75$	N/A	<1500	<100	JAEA	Upper left of Fig. 10
300,000	0–100	10	N/A	N/A	N/A	<100	JAEA	Upper right of Fig. 10
300,000	0–100	10	$A = 2.98 \times 10^{-5}$, $B = 0.75$	N/A	<3000	<100	JAEA	Middle left of Fig. 10
300,000	0–100	10	$A = 8.40 \times 10^{-5}$, $B = 0.79$	N/A	<1500	<100	JAEA	Middle right of Fig. 10
300,000	0–100	10	$A = 2.98 \times 10^{-5}$, $B = 0.75$	N/A	<1500	<40	JAEA	Lower-left of Fig. 10
100,000	0–100	10	$A = 2.98 \times 10^{-5}$, $B = 0.75$	N/A	<1500	<100	JAEA	Lower right of Fig. 10
300,000	0–100	5	$A = 2.98 \times 10^{-5}$, $B = 0.75$	$A = 2.98 \times 10^{-5}$, $B = 0.30$	<1500	<100	JAEA2	Upper panels of Fig. 13
300,000	0–100	10	$A = 2.98 \times 10^{-5}$, $B = 0.75$	N/A	<1500	<100	JAEA2	Lower-left of Fig. 13

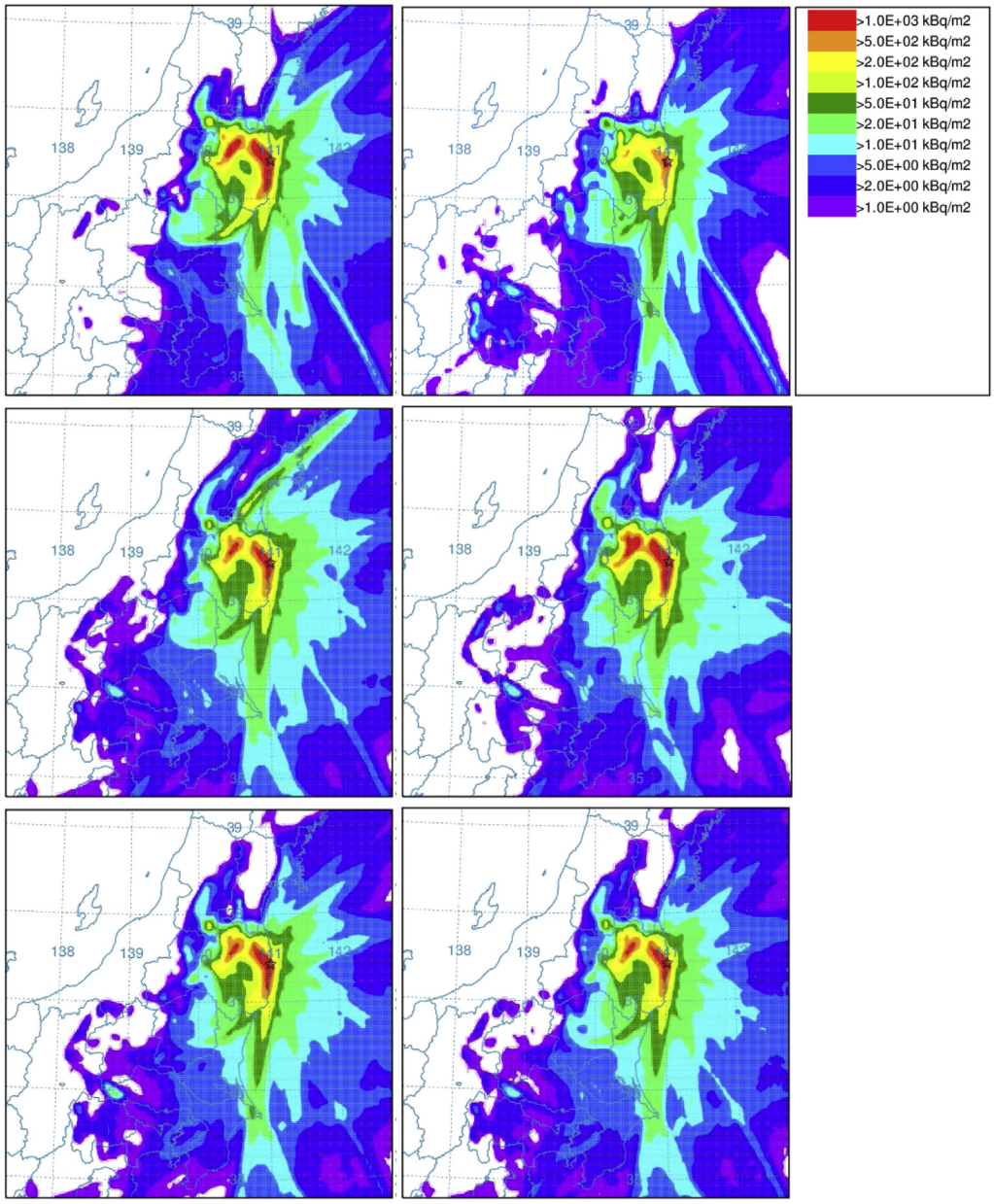

Fig. 10. Same as in the lower-left panel of Fig. 7, but following settings are different: Upper left: for the case with the release height of 0–30 m AGL. Upper right: for the case without wet scavenging. Middle left: for the case with wet scavenging below 3000 m. Middle right: for the case with the below-cloud scavenging coefficient of $\Lambda_w = 8.40 \times 10^{-5} P^{0.79}$. Lower left: for the case with dry deposition application height $Z_d = 40$ m. Lower right: for the case with the number of tracer $N = 100{,}000/3$ h.

values are plotted, the regions dominated by dry deposition. As seen in this figure, the area with high deposition in the northwest of Fukushima DNPP and the hotspot at 'Naka-dori' were primarily formed by wet scavenging by snow and rain (Fig. 4) influenced by the orographic effect of the O'u mountain range.

5.3. SCJ Model intercomparisons and further revisions of RATM

The SCJ reviewed the modeling capability of the transportation of radioactive materials released to the environment as a result of the Fukushima DNPP accident. The primary purpose of this initiative was to assess the uncertainties in the ATDM results through model intercomparisons (Takigawa et al., 2013). In participating in these model intercomparisons, we further modified JMA-RATM as noted by the following three points:

(i) The revised release rate 'JAEA2' by Kobayashi et al. (2013) (solid line in Fig. 6) was used.
(ii) The time step of the Lagrangian trace advection was changed from 10 min to 5 min.
(iii) The precipitation rate of solid waters (snow and graupel) in the JMA-MESO analysis was used for wet scavenging in addition to that of rain.

The model outputs were converted to GrADS format as requested by SCJ.

We assumed the scavenging coefficients in Eq. (1) for snow to have the same value for A, and used 0.30 for B with reference to the value of UKMET-NAME (Leadbetter et al., 2014). Fig. 12 shows the relationship between below-cloud scavenging coefficients and precipitation intensity. For the in-cloud scavenging rate of ^{131}I, Eq. (3) was employed without modification.

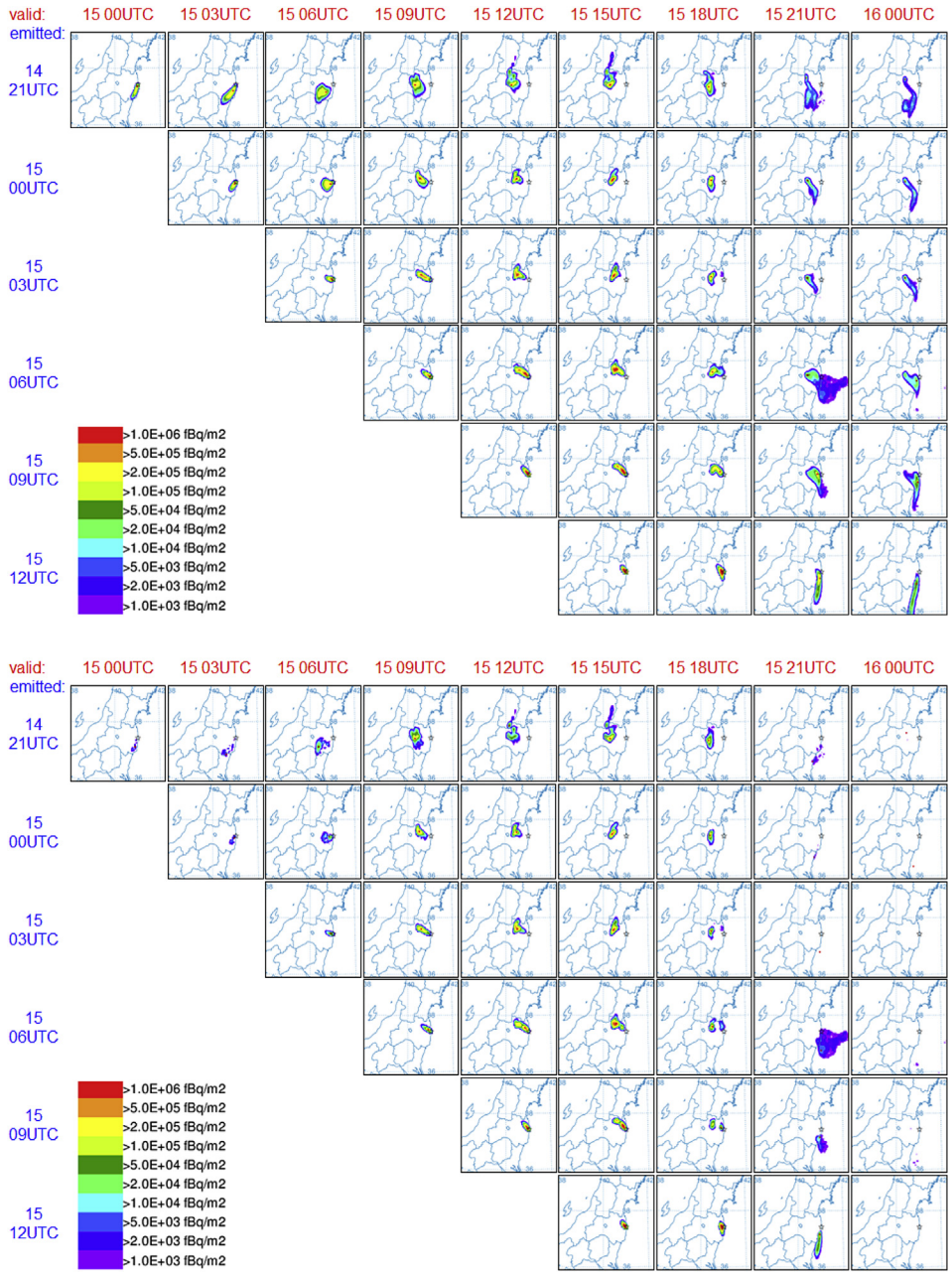

Fig. 11. Three-hourly ^{137}Cs deposition at each valid time with unit release for 14 March 2100 UTC–15 March 1200 UTC. Upper: total deposition of dry and wet. Lower: effect of wet scavenging (difference between wet scavenging off and on).

Fig. 13 shows the ^{137}Cs deposition distribution obtained by the SCJ experiment. As seen in its enlarged view (upper right panel), the area with high deposition northwest of Fukushima DNPP is more enhanced relative to the earlier JMA-RATM results and linked with the hotspot at 'Naka-dori', producing an inverse L-shaped pattern. Since JAEA2 release rate is somewhat larger than that of JAEA (Fig. 6), the enhancement of deposition was partly caused by the change of the release rate, while the modification of treatment of the wet scavenging (use of solid waters in JMA-MESO) likely contributed to modifying the shape of the area with high deposition. It is noteworthy that in this experiment, a small hotspot in the Chiba prefecture (northeast of Tokyo, see Fig. 4 of Draxler et al., 2013) is better simulated compared with the original RATM simulation (the lower-left panel of Fig. 7).

To differentiate the impact of changes to the emission rate and model, we conducted additional experiments. The lower-left panel of Fig. 13 is for the case when only the release rate is changed to JAEA2 source term with application of below-cloud scavenging only to rain (the same model that in the lower-left panel of Fig. 7). As indicated by these figures, both changes contribute to enhance the inverse L-shaped area with high deposition, however the change of the source term has a larger effect than inclusion of snow in the below-cloud scavenging in terms of the deposition distribution over the Kanto Plain.

Another experiment with in-cloud scavenging for aerosol particles was conducted to test its impact. In this experiment, the 3-dimensional distribution of cloud water analyzed by MESO 4D-VAR was used to define cloud area and liquid water content (Eq.

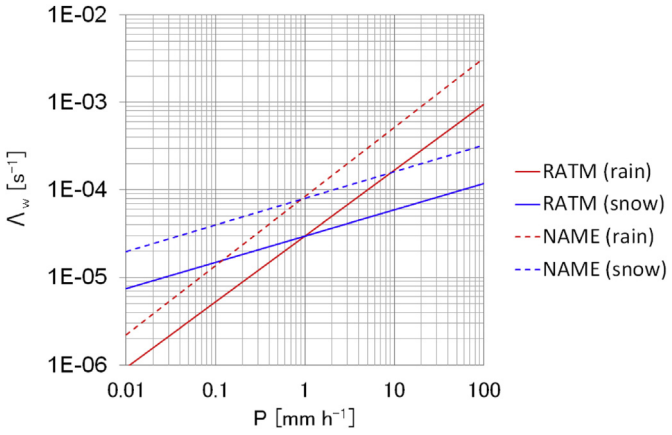

Fig. 12. Below-cloud scavenging coefficients for rain (red) and snow and graupel (blue) used in JMA-RATM for SCJ model intercomparison. Coefficients in UKMET-NAME are plotted by broken lines for reference. (For interpretation of the references to color in this figure legend, the reader is referred to the web version of this article.)

(13) of Hertel et al., 1995). The lower right panel of Fig. 13 shows the result when in-cloud scavenging of aerosol particles is considered. A very large difference is seen in the north of Kanto Plain. An area with high deposition extends from the eastern part of Fukushima prefecture to west-southwest, resembling the observed hotspot in the northern Kanto Plain (Fig. 4 of Draxler et al., 2013). Although the simulated area with high deposition has a small (20–30 km) southward positional lag, this result suggests importance of considering in-cloud scavenging for aerosol particles.

6. Summary and concluding remarks

JMA provided MESO analysis and RAP data with a file converter kit to the WMO Task Team and UNSCEAR. These data are available to the research community. The regional transport model of JMA was modified to an ATDM appropriate for the treatment of radionuclides, and further revised to more appropriately use the MESO analyses and RAP data. Verification against observations showed that the performance of JMA-RATM was significantly improved by the revision. Use of RAP data improved the ^{137}Cs deposition pattern while it degraded the time series of concentration at the JAEA observation site. The reason of this deterioration is not obvious, but a similar tendency was found in the other Task Team's ATDM experiments. The discrepancy of the transport patterns produced by the NWP analyses with the locations of the actual precipitation areas, the quality of the RAP data and its treatment in the ATDMs, and sensitivity of time series observation at Tokai-mura to the small uncertainties in the wind direction may all affect the final results. Further investigation is required to elucidate the reason of this deterioration.

The deposition of radionuclides on March 15th was examined using the RATM simulation. Two processes contributed to the hotspot at 'Naka-dori', central part of the Fukushima prefecture; the northward secondary deposition from radionuclides released from 14th 2100 UTC to 15th 0000 UTC, and the large emission of radionuclides released from 0300 UTC to 0900 UTC of the 15th directly transported from the Fukushima DNPP. Wet scavenging as well as the blocking effect of the O'u mountain range were critical for both processes. Results of the simulations were generally not so sensitive to small changes of RATM parameters, but in the regions

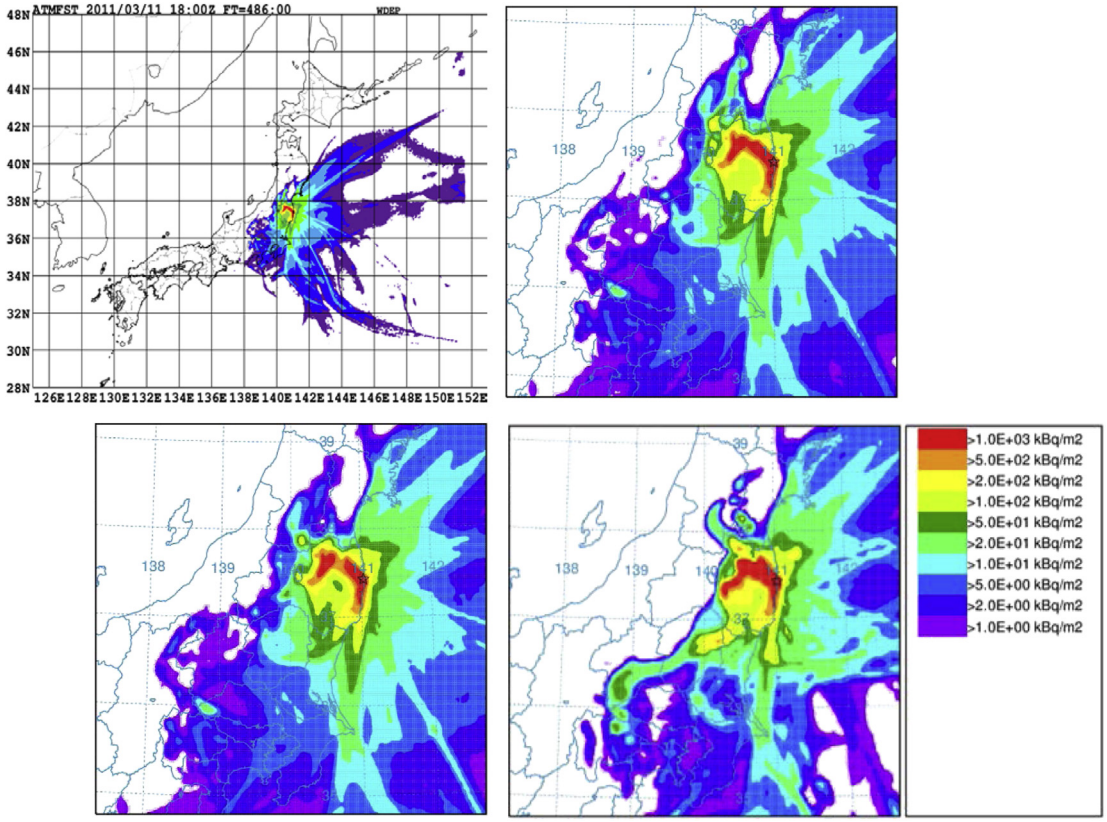

Fig. 13. Upper left: distribution of ^{137}Cs deposition by JMA-RATM in the SCJ model intercomparison. Upper right: same as in the upper left figure but enlarged view for the same domain as in the lower-left panel of Fig. 7. Lower left: same as in the lower left panel of Fig. 7 (below-cloud scavenging is applied only to rain) but for the case that the release rate is given by JAEA2. Lower right: same as in the upper right figure but for a preliminary test case that in-cloud scavenging for aerosol particles is roughly considered.

with weak deposition, a lower release height (30 m) and a lower wet scavenging application height (1500 m) yielded slightly better results compared with the original ones.

For the SCJ model intercomparison, further revision of JMA-RATM was made in the treatment of wet scavenging of aerosol particles, where total precipitation including solid waters in MESO was used. The area with high deposition northwest of Fukushima DNPP became more distinct, and linked with the hotspot at 'Naka-dori'. A small hotspot in the Chiba prefecture was also better simulated in the SCJ experiment. When in-cloud scavenging is considered, an area with high deposition extends from the eastern part of Fukushima prefecture to west-southwest, which resembles the observed hotspot in the northern Kanto Plain.

In the Task Team experiment, we used three-hourly MESO analysis as the meteorological field with linear interpolation in time and space to obtain input data for RATM at every 10 (or 5) min time step. The time interval of the meteorological field may not be sufficient to properly treat the upward motion of the radionuclides and to characterize their finer spatiotemporal scale transport due to changes of the wind speed and direction. To obtain more temporally resolved meteorological fields, additional mesoscale model simulations would be needed.

Use of a lower below-cloud scavenging application height (1500 m) yielded slightly better results in the revised version in terms of reducing the inappropriate deposition in the Miyagi prefecture, but the same effect could be obtained by reducing the scavenging coefficient itself, or changing the source emissions. In the additional experiment for the SCJ case, we tested the impact of a preliminary in-cloud scavenging scheme for aerosol particles, and the result suggested the importance of its consideration. More sophisticated method should be developed for in-cloud scavenging so that the 3-dimensional distribution of rain in the MESO analysis can be used more effectively. In addition, changes of the assumed particle size distribution with a mean diameter (1 μm) and a uniform particle density (1 g cm^{-3}) will also have an effect on the surface deposition. These points are all subjects for future research.

Acknowledgments

We thank members of the WMO technical task team, Matthew Hort of UK Met Office, René Servranckx and Alain Malo of Canadian Meteorological Center, and Gerhard Wotawa of ZAMG, for their great effort and contributions to the task team. We also thank Peter Chen of the WMO Secretariat for taking the initiative to organize the task team activities, and Masamichi Chino of the Japan Atomic Energy Agency for providing source term and air concentration measurement data. JMA-MESO and RAP data and the file converter kit were provided by Teruyuki Kato, Tabito Hara, Eiji Toyoda and Tsukasa Fujita of the Numerical Prediction Division of the Japan Meteorological Agency. Thanks are extended to Kazuhiko Nagata, Yuki Honda, Naoyuki Hasegawa and Tatsuya Kimura of the Office of International Affairs of the Japan Meteorological Agency for their help and understandings. We are indebted to Taichu Tanaka of the Meteorological Research Institute of JMA for his help on the SCJ model intercomparison. Valuable comments by Mark Cohen and Fong Ngan of the Air Resources Laboratory of NOAA and two anonymous reviewers significantly improved the quality of the manuscript.

This study was partly supported by the Ministry of Education, Culture, Sports, Science and Technology of Japan through the Grant-in-Aid for Scientific Research (24340115) and the Field 3 of the Strategic Programs for Innovative Research (SPIRE), 'Ultra high accuracy mesoscale weather prediction'.

References

Arnold, D., Maurer, C., Wotawa, G., Draxler, R., Saito, K., Seibert, P., 2014. Influence of the meteorological input on the local and global atmospheric transport of radionuclides after the Fukushima Daiichi nuclear accident. J. Environ. Radioact. 139, 212–225.

Chen, P., Draxler, R., Hort, M., Saito, K., Wotawa, G., 2011. Meeting of the WMO Task Team on Meteorological Analyses for Fukushima Daiichi Nuclear Power Plant Accident. WMO CBS Report, p. 27. Available online at. http://www.wmo.int/pages/prog/www/CBS-Reports/documents/FinalRep_TT_FDnpp_v6.pdf.

Chen, P., Draxler, R., Hort, M., Saito, K., Wotawa, G., 2012a. Second Meeting of the WMO Task Team on Meteorological Analyses for Fukushima Daiichi Nuclear Power Plant Accident. WMO CBS Report, p. 13. Available online at. http://www.wmo.int/pages/prog/www/CBS-Reports/documents/FinalReport_TTMetAnalyFDnpp.pdf.

Chen, P., Draxler, R., Hort, M., Saito, K., Wotawa, G., 2012b. Third Meeting of the WMO Task Team on Meteorological Analyses for Fukushima Daiichi Nuclear Power Plant Accident. WMO CBS Report, p. 9. Available online at: http://www.wmo.int/pages/prog/www/CBS-Reports/documents/FINAL-REPORT.pdf.

Chino, M., Nakayama, H., Nagai, H., Terada, H., Katata, G., Yamazawa, H., 2011. Preliminary estimation of release amounts of 131I and 137Cs accidentally discharged from the Fukushima Daiichi nuclear power plant into the atmosphere. J. Nucl. Sci. Technol. 48, 1129–1134. http://dx.doi.org/10.1080/18811248.2011.9711799.

Draxler, R.R., 2006. The Use of global and mesoscale meteorological model data to predict the transport and dispersion of tracer plumes over Washington, D.C. Weather Forecast. 21 (3), 383–394. http://dx.doi.org/10.1175/WAF926.1.

Draxler, R.R., Rolph, G.D., 2012. Evaluation of the transfer coefficient matrix (TCM) approach to model the atmospheric radionuclide air concentrations from Fukushima. J. Geophys. Res. 117, 10. http://dx.doi.org/10.1029/2011JD017205.

Draxler, R., Arnold, D., Galmarini, S., Hort, M., Jones, A., Leadbetter, S., Malo, A., Maurer, C., Rolph, G., Saito, K., Servranckx, R., Shimbori, T., Solazzo, E., Wotawa, G., 2013. Evaluation of Meteorological Analyses for the Radionuclide Dispersion and Deposition from the Fukushima Daiichi Nuclear Power Plant Accident. In: WMO Technical Publication, 1120, p. 64. Available online at: https://www.wmo.int/e-catalog/detail_en.php?PUB_ID=669.

Draxler, R., Arnold, D., Chino, M., Galmarini, S., Hort, M., Jones, A., Leadbetter, S., Malo, A., Maurer, C., Rolph, G., Saito, K., Servranckx, R., Shimbori, T., Solazzo, E., Wotawa, G., 2014. World meteorological organization's model simulations of the radionuclide dispersion and deposition from the Fukushima Daiichi nuclear power plant accident. J. Environ. Radioact. 139, 172–184.

Gifford, F.A., 1982. Horizontal diffusion in the atmosphere: a Lagrangian-dynamical theory. Atmos. Environ. 16, 505–512.

Gifford, F.A., 1984. The random force theory: application to meso and large-scale atmospheric diffusion. Bound.-Layer Meteor. 30, 159–174.

Hertel, O., Christensen, J., Runge, E.H., Asman, W.A.H., Berkowicz, R., Hovmand, M.F., 1995. Development and testing of a new variable scale air pollution model – ACDEP. Atmos. Environ. 29, 1267–1290.

Honda, Y., Nishijima, M., Koizumi, K., Ohta, Y., Tamiya, K., Kawabata, T., Tsuyuki, T., 2005. A pre-operational variational data assimilation system for a non-hydrostatic model at the Japan meteorological agency: formulation and preliminary results. Q. J. Roy. Meteorol. Soc. 131, 3465–3475.

Honda, Y., Sawada, K., 2008. A new 4D-Var for mesoscale analysis at the Japan meteorological agency. CAS/JSC WGNE Res. Act. Atmos. Ocean Model. 38, 01.7–01.8.

Iwasaki, T., Maki, T., Katayama, K., 1998. Tracer transport model at Japan meteorological agency and its application to the ETEX data. Atmos. Environ. 32, 4285–4295.

JMA, 2012. Users' Manual of Conv Jma Grib2—a Tool to Convert GRIB2 provided for UNSCEAR by JMA, p. 8. Available online with permission of WMO at: http://www.wmo.int/metdata1/.

Kinoshita, N., Sueki, K., Sasa, K., Kitagawa, J., Ikarashi, S., Nishimura, T., Wong, Y., Satou, Y., Handa, K., Takahashi, T., Sato, M., Yamagata, T., 2011. Assessment of individual radionuclide distributions from the Fukushima nuclear accident covering central-east Japan. Proc. Natl. Acad. Sci. U. S. A., 4. http://dx.doi.org/10.1073/pnas.1111724108.

Kitada, T., 1994. Modelling of transport, reaction and deposition of acid rain. Kishou Kenkyu Note 182, 95–117 (in Japanese).

Kobayashi, T., Nagai, H., Chino, M., Kawamura, H., 2013. Source term estimation of atmospheric release due to the Fukushima Dai-ichi Nuclear Power Plant accident by atmospheric and oceanic dispersion simulations. J. Nucl. Sci. Technol. 50, 255–264. http://dx.doi.org/10.1080/00223131.2013.772449.

Koizumi, K., Ishikawa, Y., Tsuyuki, T., 2005. Assimilation of precipitation data to JMA mesoscale model with a four-dimensional variational method and its impact on precipitation forecasts. SOLA Sci. Online Lett. Atmosphere) 1, 45–48.

Leadbetter, S., Hort, M., Jones, A., Webster, H., Draxler, R., 2014. Sensitivity of the deposition of Caesium-137 from Fukushima Dai-ichi nuclear power plant on the wet deposition parameterisation in NAME. J. Environ. Radioact. Special Fukushima issue (condionally accepted).

Louis, J.F., Tiedtke, M., Geleyn, J.F., 1982. A short history of the operational PBL parameterization at ECMWF. In: Workshop on Planetary Boundary Layer Parameterization. ECMWF, pp. 59–79.

MEXT, 2011. Preparation of Distribution Map of Radiation Doses, Etc. (Map of Radioactive Cesium Concentration in Soil) by MEXT. Available online at: http://radioactivity.nsr.go.jp/en/contents/5000/4165/24/1750_083014.pdf.

Morino, Y., Ohara, T., Nishizawa, M., 2011. Atmospheric behavior, deposition, and budget of radioactive materials from the Fukushima Daiichi nuclear power plant in March 2011. Geophys. Res. Lett. 38, L00G11. http://dx.doi.org/10.1029/2011GL048689.

Nagata, K., 2011. Quantitative precipitation estimation and quantitative precipitation forecasting by the Japan meteorological agency. In: RSMC Tokyo – Typhoon Center Technical Review, 13, pp. 37–50. Available online at: www.jma.go.jp/jma/jma-eng/jma-center/rsmc-hp-pub-eg/techrev/text13-2.pdf.

Saito, K., Fujita, T., Yamada, Y., Ishida, J., Kumagai, Y., Aranami, K., Ohmori, S., Nagasawa, R., Kumagai, S., Muroi, C., Kato, T., Eito, H., Yamazaki, Y., 2006. The operational JMA nonhydrostatic mesoscale model. Mon. Weather Rev. 134, 1266–1298.

Saito, K., Ishida, J., Aranami, K., Hara, T., Segawa, T., Narita, M., Honda, Y., 2007. Nonhydrostatic atmospheric models and operational development at JMA. J. Meteor. Soc. Jpn. 85B, 271–304.

Saito, K., 2012. The Japan meteorological agency nonhydrostatic model and its application to operation and research. In: Atmospheric Model Applications. InTech, pp. 85–110. http://dx.doi.org/10.5772/35368.

Saito, K., Shimbori, T., Hara, T., Toyoda, E., Kato, T., Fujita, T., Nagata, K., Honda, Y., 2014. JMA's Contribution to the WMO Technical Task Team on Meteorological Analyses for Fukushima Daiichi Nuclear Power Plant Accident. Open access bulletin of JMA's business reports in Japanese,. Sokko-jiho (in press). Available online at: http://www.jma.go.jp/jma/kishou/books/sokkou/sokkou.html.

Seino, N., Sasaki, H., Sato, J., Chiba, M., 2004. High-resolution simulation of volcanic sulfur dioxide dispersion over the Miyake Island. Atmos. Environ. 38, 7073–7081.

Shimbori, T., Aikawa, Y., Seino, N., 2009. Operational implementation of the tephra fall forecast with the JMA mesoscale tracer transport model. CAS/JSC WGNE Res. Act. Atmos. Ocean. Model. 39, 5.29–5.30.

Shimbori, T., Aikawa, Y., Fukui, K., Hashimoto, A., Seino, N., Yamasato, H., 2010. Quantitative tephra fall prediction with the JMA mesoscale tracer transport model for volcanic ash: a case study of the eruption at Asama volcano in 2009. Pap. Met. Geophys. 61, 13–29. http://dx.doi.org/10.2467/mripapers.61.13 (in Japanese with English abstract and figure captions).

Sportisse, B., 2007. A review of parameterizations for modelling dry deposition and scavenging of radionuclides. Atmos. Environ. 41, 2683–2698.

Suzuki, T., 1983. A theoretical model for dispersion of tephra. In: Shimozuru, D., Yokoyama, I. (Eds.), Arc Volcanism: Physics and Tectonics. TERRAPUB, Tokyo, pp. 95–113.

Takano, I., Aikawa, Y., Gotoh, S., 2007. Improvement of photochemical oxidant information by applying transport model to oxidant forecast. CAS/JSC WGNE Res. Act. Atmos. Ocea. Model. 37, 5.35–5.36.

Takigawa, M., Nagai, H., Morino, Y., Sekiyama, T., Hayami, H., Tanaka, T., Nakajima, T., Shibata, T., 2013. International intercomparison of atmospheric simulations of radionuclides. In: Proceedings of the 54th Annual Meeting of Japan Society for Atmospheric Environment, p. 136 (in Japanese).

Terada, H., Katata, G., Chino, M., Nagai, H., 2012. Atmospheric discharge and dispersion of radionuclides during the Fukushima Dai-ichi Nuclear Power Plant accident. Part II: verification of the source term and analysis of regional-scale atmospheric dispersion. J. Environ. Radioact. 112, 141–154. http://dx.doi.org/10.1016/j.jenvrad.2012.05.023.

Toyoda, E., 2012. Radar/Rain Gauge-Analyzed Precipitation Dataset by JMA, p. 11. Available from JMA.

USDOE, 2011. United States Department of Energy. https://explore.data.gov/Geography-and-Environment/US-DOE-NNSA-Response-to-2011-Fukushima-Incident-Ra/prrn-6s35.